View metadata, citation and similar papers at core.ac.uk
brought to you by CORE
provided by Ghent University Academic Bibliography

# Split-Bregman-based sparse-view CT reconstruction

Bert Vandeghinste, Bart Goossens, Jan De Beenhouwer, Aleksandra Pizurica, Wilfried Philips, Stefaan Vandenberghe and Steven Staelens

***Abstract*—Total variation minimization has been extensively researched for image denoising and sparse view reconstruction. These methods show superior denoising performance for simple images with little texture, but result in texture information loss when applied to more complex images. It could thus be beneficial to use other regularizers within medical imaging. We propose a general regularization method, based on a split-Bregman approach. We show results for this framework combined with a total variation denoising operator, in comparison to ASD-POCS. We show that sparse-view reconstruction and noise regularization is possible. This general method will allow us to investigate other regularizers in the context of regularized CT reconstruction, and decrease the acquisition times in $\mu$CT.**

***Index Terms*—Computed Tomography, Iterative Algorithms, Noise, Reconstruction Algorithms**

## I. Introduction

In in-vivo $\mu$CT, a research topic emerging in the last years is dual-energy or spectral energy imaging. The decomposition methods are however highly susceptible to the high noise in the $\mu$CT images. Also, due to the extra binning in spectral CT detectors, the detector noise will increase even more. Overcoming this issue with longer acquisition times is impossible due to limitations on administered dose and anesthetics in in-vivo small animal imaging. Reducing the number of acquisition angles and the overall noise through reconstruction means may provide us with the perfect tools for in-vivo spectral $\mu$CT.

Total variation (TV) minimization is one of the techniques that have been extensively researched in the last decade in the context of image denoising by image processing groups [1]. In the context of compressed sensing, TV minimization was used for few-view and limited-angle CT reconstruction [2]–[6], as well as sparse-view MRI reconstruction [7]. All implementations of these ideas share the same basic framework as in [2].

This work was supported in part by a PhD grant to Bert Vandeghinste of the Institute for the Promotion of Innovation through Science and Technology in Flanders (IWT-Vlaanderen) and by the CIMI project, an IBBT-project in cooperation with: Barco nv, DCILABS, IBA Dosimetry, GE and DSC Labs. IBBT is an independent multidisciplinary research institute founded by the Flemish Government, to stimulate ICT innovation. *Asterisk indicates corresponding author.*

*B. Vandeghinste, J. De Beenhouwer, S. Vandenberghe and S. Staelens are with the Medical Image and Signal Processing (MEDISIP) research group, Ghent University–IBBT, 9000 Gent, Belgium. (e-mail: bert.vandeghinste@ugent.be).

B. Goossens is a postdoctoral research fellow with FWO, Flanders. He, A. Pizurica and W. Philips are with the Image Processing and Interpretation (IPI) research group, Ghent University–IBBT, Sint-Pietersnieuwstraat 41, 9000 Gent, Belgium.

J. De Beenhouwer is also with The Vision Lab, University of Antwerp, 2610 Wilrijk, Belgium.

S. Staelens is also with the Molecular Imaging Centre Antwerp, University of Antwerp, 2650 Edegem, Belgium.

It is generally understood that TV-based methods have superior denoising performance when applied to simple classes of images with no textures, such as images of conic shapes with flat colors. These methods, however, often produce approximations that are reminiscent of cartoons when applied to images that contain complex textures and shading. This can be understood by considering [1] in a Bayesian framework. Data fidelity expresses the likelihood, while TV models the prior on the denoised image. Piecewise constant images have a low TV and are given a high probability. TV minimization therefore biases the solution towards piecewise constant (cartoon like) images. This is also referred to as the staircasing effect [8]–[10]. The TV regularizer is thus unsuitable for medical images with complex textures, such as those in CT.

We propose a general regularization method, based on the split-Bregman approach [11], as a different method for sparse-view CT reconstruction. As stated in [11], the most significant advantage of the Bregman iteration technique, is that the convergence speed can be chosen optimally by the user. Ultimately, we want to use this technique with regularizers different from TV. As a means of validation however, we chose to present this technique using TV. We call this SpBR-TV.

The remainder of this paper is organized as follows. In Section II, we introduce the problem formulation and the mathematical background for using the split-Bregman approach in CT. Section III describes the set-up for the simulation data for a Shepp-Logan phantom and the in-vivo measured $\mu$CT data. Section IV contains the results, comparing Simultaneous Iterative Reconstruction Technique (SIRT) [12], [13] and adaptive-steepest-descent projection-on-convex-sets (ASD-POCS) [6] with SpBR, using TV as regularizer. These results are then discussed in section V. Finally, we conclude in section VI.

## II. Preliminaries

### A. Noise free case

In the noise free case, the projection data $y$ is modeled by

$$y_i = \sum_{j=1}^{N} w_{ij} x_j, \tag{1}$$

where the weights $w_{ij}$ incorporate some approximations of the forward projection model. Equation (1) can alternatively be written in matrix-form as

$$\mathbf{y} = \mathbf{W}\mathbf{x}, \tag{2}$$

with $w_{ij}$ the elements of $\mathbf{W}$.

With no noise present and an underdetermined system (less projection samples than pixels in the image), solving for $\mathbf{x}$ gives the following cost function:

$$g(\mathbf{x}) = ||\mathbf{y} - \mathbf{W}\mathbf{x}||_2^2. \tag{3}$$

The optimal solution is then given by the pseudoinverse. Unfortunately, this pseudoinverse is too complicated to compute directly in CT imaging. An alternative is using gradient descent steps:

$$\frac{\partial g(\mathbf{x})}{\partial \mathbf{x}} = -2\mathbf{W}^T(\mathbf{y} - \mathbf{W}\mathbf{x}) \tag{4}$$

such that

$$\mathbf{x}^{(i+1)} = \mathbf{x}^{(i)} + 2\lambda\mathbf{W}^T(\mathbf{y} - \mathbf{W}\mathbf{x}^{(i)}) \tag{5}$$

with $(i)$ the iteration number.

Assuming that the row sum and column sum are 1 and $\lambda = 1/2$ and correct scaling, this gives the classical SIRT algorithm [12], [13]. The gradient descent algorithm will converge to the pseudoinverse.

### *B. In the presence of noise*

When noise is present in sinogram space, we have the good additive approximation:

$$\mathbf{y} = \mathbf{W}\mathbf{x} + \mathbf{n} \tag{6}$$

with $\mathbf{n}$ given by a Gaussian Random Field [14]. Because the noise is zero-mean by approximation, the data fitting function (3) is still applicable, except for a diagonal matrix $\mathbf{C}$. This matrix can model detector acquisition system, such as the noise variances for each projection sample or the correlations between different detector elements. However, because the problem is very ill-posed (noisy data and/or sparse views), we will need to use regularization to properly reconstruct the CT image.

Therefore, we will use the following cost criterium:

$$\hat{\mathbf{x}} = \arg\min_{\mathbf{x}} |\Phi(\mathbf{x})|_1 + \lambda||\mathbf{C}^{-1/2}(\mathbf{y} - \mathbf{W}\mathbf{x})||_2^2, \tag{7}$$

with $\Phi$ a sparsifying transformation (e.g. the gradient images in the X, Y and Z directions for TV) and with $\mu$ constant.

This can be efficiently solved using augmented Lagrangian approaches. Reference [11] shows that the generalized constrained optimization problem

$$\min_{\mathbf{x}} E(\mathbf{x}) \quad s.t. \quad \mathbf{y} = \mathbf{W}\mathbf{x} \tag{8}$$

can be solved by iterating over

$$\mathbf{x}^{(i+1)} = \min_{\mathbf{x}} E(\mathbf{x}) + \frac{\lambda}{2}||\mathbf{W}\mathbf{x} - \mathbf{b}^{(i)}||_2^2 \tag{9a}$$

$$\mathbf{b}^{(i+1)} = \mathbf{b}^{(i)} + \mathbf{y} - \mathbf{W}\mathbf{x}^{(i)}. \tag{9b}$$

The error in the constraint is simply added back to the right hand side. This is equivalent to "adding the noise back" in the Rudin-Oshir-Fatemi (ROF) model for TV denoising [1].

In [11] is is then shown, provided (9a) and (9b) converge in the sense of

$$\lim_{i\to\infty} \mathbf{W}\mathbf{x}^{(i)} = \mathbf{y}, \tag{10}$$

that the iterates $x^{(i)}$ will get arbitrarily close to a solution of the original constrained problem (8).

Applying (9a) and (9b) to (7) leads to the following 3 update equations:

$$\mathbf{x}^{(i+1)} = \arg\min_{\mathbf{x}} \frac{\lambda}{2}||\mathbf{C}^{-1/2}(\mathbf{y} - \mathbf{W}\mathbf{x})||_2^2 + \frac{\mu}{2}||\mathbf{d}^{(i)} - \Phi(\mathbf{x}) - \mathbf{b}^{(i)}||_2^2 \tag{11a}$$

$$\mathbf{d}^{(i+1)} = \arg\min_{\mathbf{d}} |\mathbf{d}|_1 + \frac{\mu}{2}||\mathbf{d} - \Phi(\mathbf{x}^{(i+1)}) - \mathbf{b}^{(i)}||_2^2 \tag{11b}$$

$$\mathbf{b}^{(i+1)} = \mathbf{b}^{(i)} + (\Phi(\mathbf{x}^{(i+1)}) - \mathbf{d}^{(i+1)}). \tag{11c}$$

The auxiliary variables $\mathbf{d}^{(0)}$ and $\mathbf{b}^{(0)}$ are initialized with $\mathbf{0}$ at the beginning of the algorithm.

The speed of the split-Bregman method is largely dependent on how fast we can solve each of the first two sub problems. This in turn depends on the specific transformations used.

To solve (11a), Gauss-Siedel or Fourier transform methods can be used, depending on the exact nature of the data fidelity term.

In (11b), there is no coupling between elements of $\mathbf{d}$. We can explicitly compute the optimal value of $\mathbf{d}$ using shrinkage operators.

We compute

$$\mathbf{d}_k^{(i+1)} = softshrink(\Phi(\mathbf{x})_k + \mathbf{b}_k^{(i)}, \frac{1}{\mu}) \tag{12}$$

with

$$softshrink(x, \gamma) = \frac{x}{|x|} \times max(|x| - \gamma, 0). \tag{13}$$

Shrinkage is an extremely fast operation, and requires only a few operations per element of $\mathbf{d}^{(i+1)}$.

Equation (11c) is trivial to solve.

Parameter $\lambda$ determines the contribution of the regularization to the total cost. The lower the value, the more the resulting reconstruction will be denoised. Parameter $\mu$ determines the convergence speed. The higher $\mu$, the faster the algorithm will converge to the solution determined by $\lambda$. The ability to choose the convergency speed is one of the main advantages of a Bregman iteration approach [11]. When these parameters are set to $\mu = 0$ and $\lambda = 1$, no regularization is performed. We then obtain the classical SIRT algorithm with cost function (3).

## III. Materials and Methods

Equations (11a–11c) were implemented in an iterative CT reconstruction framework developed at our research group. Conjugate Gradient on the Normal Equations (CGNE) was used to implement (11a). This optimization method uses $\mathbf{W}$, the forward projector, and $\mathbf{W}^T$, the backward projector, to solve $\mathbf{y} = \mathbf{W}\mathbf{x}$. These were implemented as Siddon ray-tracers [15]. The stopping condition for CGNE was fulfilled when the squared l2-norm of the new residual got below some pre-defined value. For noiseless simulation tests we set this tolerance at $1 \times 10^{-7}$. This leads to less than 100 CGNE iterations. The $\mathbf{C}$ parameter was set to the identity matrix.

The parameters $\mu$ and $\lambda$ were empirically chosen based on a pre-test. This involved solving (11a-11c) using the identity matrix $\mathbf{I}$ for $\mathbf{W}$, and $\mathbf{x}$ set to the reconstructed image obtained

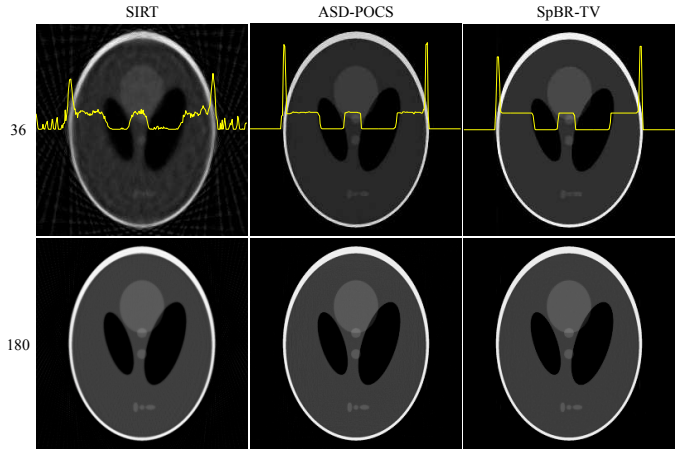


Fig. 1. Comparison between SIRT, ASD-POCS and our new method for 36 angles and for 180 angles. In the top row, a line profile has been plotted through the central row. Window [0, MAX].

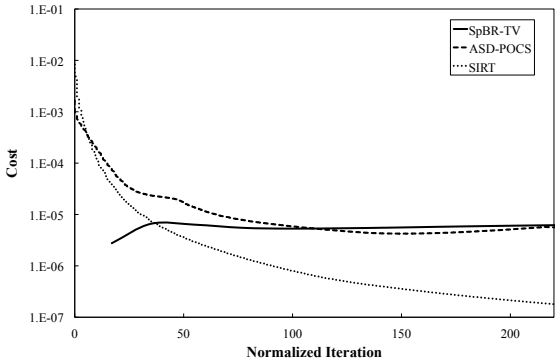


Fig. 2. Cost of the different methods plotted against the iteration number. As cost the data fitting error $||y - Wx||_2^2$ was used, normalized over the total number of elements. Only the outer iterations have been plotted, normalized to the complexity of one iteration.

from setting $\mu = 0$ and $\lambda = 1$. This amounts to pure de-noising and allows to investigate the different possibilities for $\lambda$.

The reconstruction algorithms were tested on simulated data from a digital Shepp-Logan phantom. The phantom was generated with a size of $1024 \times 1024$ pixels. The imaging detector was modeled as a line of $2368$ elements. X-ray projections were then generated by ray-tracing using Siddon along $36$ and $180$ angles over a $2\pi$ rotation. To help reduce redundancy in the projection data, the second half of the angular measurements ($180°$ to $360°$) was shifted by half the angular spacing. These projections were then used as input to the reconstruction algorithms.

The measured data were obtained from a flat-panel cone-beam $\mu$CT scanner during an in-vivo contrast-enhanced mouse scan. The detector exists of $1280 \times 1120$ elements with a $100\mu m$ pixel pitch. $2048$ views were obtained. This data was reconstructed to a $256^3$-grid with a voxel size of 0.1 mm. We rebinned the $2048$ views to $64$ views by keeping only every 32th projection, to obtain a sparse-view dataset.

## IV. Results

Fig. 1 shows different converged solutions for SIRT, ASD-POCS and SpBR-TV, for 36 angles and for 180 angles. For SpBR-TV, $50.0$ was empirically chosen for both $\mu$ and $\lambda$. $C$ was set to the identity matrix, effectively canceling its effect. The $\epsilon$-parameter for ASD-POCS was then chosen at $\epsilon = 25.0$ to get a comparable visual quality to the SpBR-TV result. A line-profile through the central row has been drawn on top of the 36-views images.

The convergence speed of these methods is plotted on Fig. 2, by evaluating the data fitting error $||\mathbf{y} - \mathbf{Wx}||_2^2$, normalized to the number of detection elements, after each outer iteration. The number of iterations has been normalized to the complexity of one iteration for the respective method.

Table I shows the normalized root mean squared error (NRMSE) and edge cross-correlation coefficient (E-CC) [16] for the 3 methods for both datasets.

Fig. 3 shows the results obtained reconstructing the measured dataset with SpBR-TV. The first image is the actual CT scan of $2048$ views, reconstructed using SIRT to convergence. The second image shows SIRT using only $64$ views. The last image shows the $64$-view dataset, reconstructed using SpBR-TV with $\mu = 100$ and $\lambda = 12$. The NRMSE has been calculated against the $2048$-view SIRT reconstruction, and plotted on top of the images.

TABLE I
NRMSE and E-CC of the different methods at convergence.

| | 36 views | | 180 views | |
|---|---|---|---|---|
| | NRMSE | E-CC | NRMSE | E-CC |
| SIRT | 0.376660 | 0.765521 | 0.107525 | 0.986950 |
| ASD-POCS | 0.230132 | 0.992087 | 0.105009 | 0.996503 |
| SpBR-TV | 0.091894 | 0.992751 | 0.063433 | 0.997580 |

## V. Discussion

It is clear on Fig. 1 that sparse-view reconstruction is possible with our method. For noiseless data, less than 36 views are necessary to get sufficient image quality. The ASD-POCS reconstructed image shows a little bit more structure in the uniform Shepp-Logan regions than the SpBR-TV reconstruction. SpBR-TV shows good convergence to a regularized solution for both the 36 angles dataset as well as the 180 angles dataset.

Both SpBR-TV reconstruction and ASD-POCS show comparable image quality on Fig. 1 and comparable cost on Fig. 2. This cost is much higher than the cost for SIRT when fully converged. This is as expected, as the regularization methods do not minimize cost (3) as such, but minimize cost (7). This adds an error to the data-fitting term, allowing better suppression of the noise and aliasing artifacts.

From Table I it is clear that both ASD-POCS and SpBR-TV converge to some regularized solution, though not the same one. This is due to the different optimization method that was used and different parameter selection.

Fig. 3 is a good example of the piecewise constant biasing due to TV minimization. The leftmost figure shows a good approximation of noiseless data in in-vivo $\mu$CT scanning. When the number of views is reduced from $2048$ to $64$ views over $360°$, it becomes clear that regular reconstruction

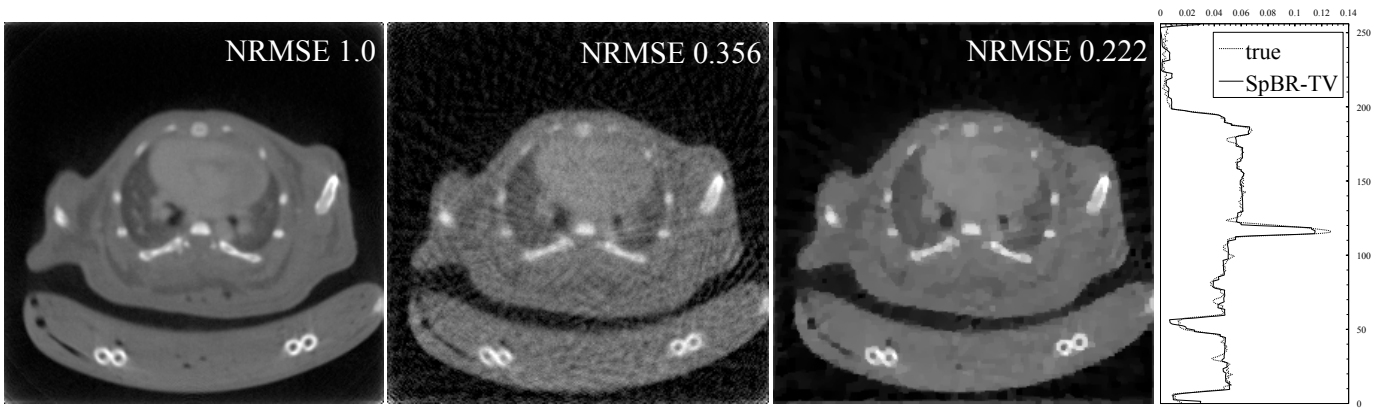


Fig. 3. Left: SIRT 2048-view reconstruction. Middle: SIRT 64-view reconstruction. Right: SpBR-TV 64-view reconstruction. NRMSE was calculated against the left-most image. Window [0, MAX]. Profile shows a vertical profile through the centre of the SIRT 2048-view reconstruction and the SpBR-TV 64-view reconstruction.

algorithms such as SIRT (middle figure) converge to a noisy solution. SpBR-TV converges to a better image, with a significant lower NRMSE, though the approximations made by TV are still visible, especially around the animal contour. The approximations are also visible on the profile, where smooth curves have been approximated by straight lines. Streaking artifacts due to bone are still apparent.

The authors want to stress that the intention of this paper was not to compare SpBR-TV and ASD-POCS as to find which one performs best. Due to parameter selection (3 parameters for SpBR-TV, 7 parameters for ASD-POCS), such a comparison would be a very strenuous task.

The advantage of our new method, is that the specific regularizer has not been incorporated from the beginning in the mathematical derivation of the split-Bregman approach for CT. This means that other regularizers or sparsifying transformations can still be used. Possible replacements for the TV regularizer are wavelets or shearlets [17], enabling simultaneous reconstruction and image denoising in multiple image resolutions. This would not bias the solution to a piecewise constant image, leading to a better regularized image than the right image in Fig. 3.

Further research will focus on optimizing this algorithm for in-vivo $\mu$CT imaging and especially for spectral $\mu$CT imaging. Sparse-view CT scanning has the potential of reducing the dose due to the smaller amount of projections scanned, reducing the total scanning time at the same time. Our focus will lay on finding better regularizers, together with a better data model in the cost function. An extensive search for the best parameters $\mu$ and $\lambda$ also needs to be conducted.

## VI. Conclusion

We have shown that a split-Bregman approach can be used to solve sparse view CT reconstruction and noise regularization. This method has been compared against conventional iterative CT reconstruction methods and one TV regularization method from literature. This general method will allow us to investigate other operators in the context of regularized CT reconstruction, and decrease the long acquisition times in $\mu$CT.

## References

[1] L. Rudin, S. sher and E. Fatemi, "Nonlinear total variation based noise removal algorithms," Physica D., vol. 60, pp. 259-268, 1992.
[2] E.Y. Sidky, C. Kao and X. Pan, "Accurate image reconstruction from few-views and limited-angle data in divergent-beam CT," Journal of X-Ray Science and Technology, vol. 14, pp. 119-139, 2006.
[3] H. Yu and G. Wang, "Compressed sensing based interior tomography," Physics in Medicine and Biology, vol. 54, pp. 2791-2805, 2009.
[4] G.T. Herman and R. Davidi, "Image reconstruction from a small number of projections," Inverse Problems, vol. 24, pp. 045001, 2008.
[5] G. Chen, J. Tang and S. Leng, "Prior image constrained compressed sensing (PICCS): A method to accurately reconstruct dynamic CT images from highly undersampled projection data sets," Medical Physics, vol. 35, pp. 660-663, 2008.
[6] E. Y. Sidky and X. Pan, "Image reconstruction in circular cone-beam computed tomography by constrained, total-variation minimization," Physics in Medicine and Biology, vol. 53, pp. 4777-4807, 2008.
[7] M. Lustig, D. Donoho and J.M. Pauly, "Sparse MRI: The application of compressed sensing for rapid MR imaging," Magnetic Resonance in Medicine, vol. 58, no. 6, pp. 1182-1195, 2007.
[8] F. Andreu, C. Ballester, V. Caselles and J.M. Mazon, "Minimizing Total Variation Flow," Differential and Integral Equations, vol. 14, no. 3, pp. 321-360, 2001.
[9] F. Andreu, V. Caselles, J.I. Diaz and J.M. Mazon, "Qualitative Properties of the Total Variation Flow", Journal of Functional Analysis, vol. 188, no. 2, pp. 516547, 2002.
[10] A. Buades, B. Coll and J. Morel, "The staircasing effect in neighborhood filters and its solution," IEEE TIP, vol. 15, no. 6, pp. 14991505, 2006.
[11] T. Goldstein and S. Osher, "The Split Bregman Method for L1 regularized problems," SIAM Journal on Imaging Sciences, vol. 2, no. 2, pp. 323- 343, 2009.
[12] P. Gilbert, "Iterative methods for the three-dimensional reconstruction of an object from projections," J. Theor. Biol., vol. 36, pp. 105-117, 1972.
[13] G.T. Herman and A. Lent, "Iterative reconstruction algorithms," Comput. Biol. Med., vol. 6, pp. 273-294, 1976.
[14] B. Goossens, "Multiresolution image models and estimation techniques," Ph.D. dissertation, Ghent University, Ghent, Belgium, 2010.
[15] R.L. Siddon, "Fast calculation of the exact radiological path for a three-dimensional CT array," Medical Physics, vol. 12, no. 2, pp. 252-255, 1985.
[16] W. Xu and K. Mueller, "Learning effective parameter settings for iterative CT reconstruction algorithms," Fully 3D Image Reconstruction in Radiology and Nuclear Medicine Conference, Beijing, China, September, 2009.
[17] G.R. Easley, D. Labate and F. Colonna, "Shearlet based total variation for denoising," IEEE TIP, vol. 18, no. 2, pp. 260-268, 2009.